OPEN ACCESS Freely available online

AFM Applied Functional Materials

ISSN 2737-5323
Issue 1
Volume 6
Applied Functional Materials

Article

Hydrogel Films Based on Alginate and Hyaluronic Acid Embedded with PCL-T Nanoparticles for Topical and Thermoresponsive Lidocaine Delivery

Rachel Faverzani Magnago [1,*], Danilo Pereira Darella [2], Thalia Viscardi Joaquim [2], Fernanda Mendes de Moraes [2], Luiz Alberto Kanis [3], Marcelo Maraschin [1], Karine Modolon Zepon [2]

[1] Graduate Program in Biotechnology and Bioscience, Federal University of Santa Catarina, Florianópolis 88034-000, Brazil; rachel.magnago@ufsc.br (R. F. M.), mtocsy@gmail.com (M. M.)
[2] Laboratory of Biomaterials and Biomimetics, University of Southern Santa Catarina, Tubarão 88701-000, Brazil; danilo.darella@gmail.com (D. P. D.), thalia_vj@outlook.com (T. V. J.), fernandamraes@gmail.com (F. M. M.), zepon.karine@gmail.com (K. M. Z.)
[3] Airela Pharmaceutica, Pedras Grandes 88720-000, Brazil; luizalbertokanis@gmail.com (L. A. K.)
* Correspondence: rachel.magnago@ufsc.br

Received: date; **Revised:** date; **Accepted:** date; **Published:** date

Abstract: This study reports the development and characterization of hydrogel films composed of alginate and hyaluronic acid, incorporating poly(ε-caprolactone-triol) (PCL-T) nanoparticles loaded with lidocaine (1%, 1.5% and 2%) for topical application. Nanoparticles were prepared via nanoprecipitation, demonstrating a high encapsulation efficiency (>99%) and thermoresponsive drug release behavior (37 ± 1°C and 43 ± 1°C). The average hydrodynamic diameters were 174 nm, 333 nm, and 920 nm, with polydispersity indices of 0.296, 0.351, and 0.172, respectively. The nanoemulsions were incorporated into a biopolymer matrix, resulting in flexible, transparent, and biocompatible films. FTIR analysis confirmed the incorporation of the nanoparticles, and mechanical testing revealed an elastic modulus comparable to that of human skin. Scanning electron microscopy revealed an increase in porosity with increasing lidocaine concentration. While the isolated nanoparticles showed thermoresponsive release, this effect was attenuated in the film matrix, potentially due to electrostatic interactions with the polyanionic alginate and hyaluronic acid. Biocompatibility was confirmed via HaCaT cell viability assays, with results indicating cell viability greater than 79%. Overall, the findings suggest that the developed films are promising candidates for sustained topical release of local anesthetics, with potential applications in wound dressings

Keywords: Thermoresponsive release, Hydrogel film, Lidocaine, PCL-T, Alginate, Sodium hyaluronate.

1. Introduction

Hydrogel films represent a class of structurally engineered materials composed of hydrophilic polymer networks, widely recognized for their ability to retain large amounts of water or fluids without dissolving, and for their versatile applications, including wound dressings and topical drug delivery systems [1,2]. Among the various types of hydrogel films, those responsive to external stimuli have attracted increasing attention in recent years [2,3]. These so-called smart hydrogel films regulate drug release through their polymer matrix, which necessitates an in-depth understanding of the physicochemical properties of the hydrogel [3], the drug, and the other formulation components [4]. Given their hydrophilic nature, incorporating hydrophobic drugs into hydrogel films often requires additional technological approaches, such as the use of micro- or nanoparticulate systems [5].

Nanotechnology involves the creation or manipulation of matter at the nanometer scale (10^{-9} metros), offering innovative solutions in the medical and pharmaceutical fields by increasing the efficacy and safety of drugs [6,7]. Nanostructured systems, such as nanospheres and nanocapsules, enhance the pharmacokinetic and pharmacodynamic profiles, thereby increasing the efficacy of existing drugs and enabling the reintroduction of previously discarded drugs due to adverse effects [6,8]. Obtaining nanoemulsions through the nanoprecipitation method is widely used because it results in a small particle size with a narrow polydispersity index [6,9–11], and especially useful for increasing the dissolution rate, apparent solubility, and permeation of lipophilic drugs through biological membranes [12].

Lidocaine [13], a local anesthetic with minimal water solubility and predominantly topical administration, is generally considered safe but may have toxic effects depending on the dose administered and the level of systemic absorption [14,15]. These

effects include, but are not limited to, central nervous system depression and respiratory failure, which can lead to death [14]. Strategies involving modified release systems have been explored to mitigate the risk of systemic overdose [16–18].

To the best of our knowledge, this is the first study to report the development of alginate and hyaluronic acid-based films incorporating polycaprolactone-triol nanoparticles (PCL-T) loaded with lidocaine, to promote sustained drug release. In this system, the lipophilic drug carrier, formed by PCL-T—a polymer widely recognized for its biocompatibility and biodegradability—is dispersed within the hydrogel matrix, conferring properties that favor its application in dressings for treating wounds with abundant exudate [19] and/or chronicles [20,21], with the potential to improve therapeutic efficacy and long-term local pain control.

Alginate, an anionic polysaccharide extracted from brown algae, stands out for its high exudate absorption capacity and the formation of hydrophilic gels through ion exchange with divalent cations, such as calcium. These properties make the material especially effective in dressings for exuding wounds, while simultaneously providing a moist, healing-friendly environment. Furthermore, alginate has hemostatic properties and can be easily combined with bioactive or antimicrobial agents, also acting as a matrix for controlled topical release [22,23]. On the other hand, hyaluronic acid (HA), a glycosaminoglycan widely distributed in the extracellular matrix of human tissues, contributes significantly to tissue regeneration through its high-water retention capacity, viscoelasticity, and interaction with cellular receptors CD44, RHAMM, and ICAM-1, which allows it to regulate adhesion, motility, inflammation, and cell differentiation. These characteristics favor cell migration, proliferation, and differentiation, which are fundamental for the processes of angiogenesis and re-epithelialization. Furthermore, HA can be chemically modified to form crosslinked hydrogels with specific mechanical properties and responses to environmental stimuli, such as pH, redox, and temperature, making it a promising material for intelligent sustained-release drug delivery systems, including intra-articular applications [24,25].

In this scenario, PCL-T, a member of the biodegradable aliphatic polyester family, also stands out, offering additional advantages over other PCL variants [17]. PCL-T has a lower melting point (~30 °C), facilitating its topical application under physiological conditions. Furthermore, it exhibits greater wettability, a faster degradation rate, and the presence of three free hydroxyl groups in its side chain, characteristics that favor interaction with hydrogels and the incorporation of active agents. Like other PCL derivatives, PCL-T is biocompatible, biodegradable, and safely metabolized by the body, either through the citric acid cycle or renal excretion. These properties make PCL-T a versatile and promising component in the formulation of advanced dressings and topical drug delivery systems, especially when combined with natural biopolymers such as alginate and hyaluronic acid [26].

The engineering of multifunctional dressings based on these biopolymers therefore represents a promising strategy in regenerative medicine and the development of materials for controlled topical drug delivery. Drug release in these systems can occur by gradual diffusion through the matrix or by matrix degradation triggered by physical or chemical stimuli, such as changes in light, pH, ionic strength, or temperature [4,27].

In thermoresponsive delivery systems, drug release is initiated by temperature variations at the site of application [4,27,28]. The unique advantage of this approach lies in its alignment with the inflammatory process, characterized by redness, swelling, pain, and localized temperature elevation. To address these symptoms, this study aims to develop an alginate/hyaluronic acid hydrogel embedded with thermoresponsive nanoparticles encapsulating anhydrous lidocaine within polycaprolactone triol for topical application.

2. Materials and Methods

2.1 Materials

Lidocaine (anhydrous form, molar mass 234.34 g/mol) was purchased from Active Pharmaceutica, sodium hyaluronate (molar mass 2,000 kDa) was obtained from Mapric, and poly(ε-caprolactone-triol) (PCL-T, molar mass 300 g/mol) was purchased from Sigma-Aldrich. Alginate was kindly provided by Danisco, with all reagents used in their original form. Acetone (99.5% purity), glycerol, calcium chloride, and Tween 80® were purchased from Labsynth. Aneuploid immortal keratinocyte (HaCat) cells were obtained from the Rio de Janeiro cell bank (Brazil). Dubellco modified Eagle's medium (DMEM), fetal bovine serum (FBS), and trypsin/EDTA solution were purchased from Sigma Aldrich (USA) and Cultilab (Brazil), respectively.

2.2 Preparation of PCL-T-based nanoemulsions

The PCL-T nanoemulsion containing lidocaine was prepared using the nanoprecipitation method, a technique based on the formation of nanoparticles from the addition of an organic phase to an aqueous phase under constant stirring, followed by the evaporation of the organic solvent [6,9,10]. Briefly, the organic phase, composed of PCL-T and different concentrations (1%, 1.5%, and 2%) of lidocaine dissolved in acetone, was slowly dripped into an aqueous phase composed of hyaluronic acid and Tween 80 at

room temperature and with constant stirring at 240 rpm [29]. After 20 min, the solution was placed in a round-bottom flask and transferred to a rotary evaporator to remove the acetone under reduced pressure and at a temperature of 40 °C. The sample coding and their respective compositions are described in Table 1.

Table 1 - Coding and composition of phases for preparation of nanoemulsions.

Codification	Organic phase			Aqueous phase		
	PCL-T (mg)	Lidocaine (mg)	Acetone (mL)	Hyaluronatede sódio (mg)	Tween 80® (mg)	Water (mL)
PCL-T:LID1%	200	200	10	30	30	20
PCL-T:LID1,5%	200	300	10	30	30	20
PCL-T:LID2%	200	400	10	30	30	20

2.3 Characterization of PCL-T-based nanoemulsions

The apparent diameter and zeta potential of the PCL-T: LID1%, PCL-T: LID1.5%, and PCL-T: LID2% nanoemulsions were determined by dynamic light scattering using a NanoBrook instrument (Brookhaven, USA). The scattered light intensity was acquired at a scattering angle of 90° with a counting time of 150 s [30].

To determine the encapsulation efficiency, 0.5 mL of PCL-T: LID1%, PCL-T: LID1.5%, and PCL-T: LID2% nanoemulsions were packaged in a filter (Amicon Ultra, cut-off 10,000 g/mol) and subsequently assembled in an Eppendorf. The filter-Eppendorf assembly was then placed in a centrifuge and subjected to centrifugation at 10,000 rpm. The fraction of unencapsulated (free) lidocaine present in the filtered sample was determined by UV-vis spectroscopy using a validated method ($R^2 = 0.996$, Equation of the straight line: $y = 2.028x - 0.0014$). Briefly, to validate the method for UV-vis quantification of lidocaine, five preparations with different concentrations (0.1, 0.2, 0.3, 0.4, and 0.5 mg/mL) were prepared and the absorbance values determined using a UV-vis spectrophotometer (UV-M51, Bel Engineering) at a wavelength of 261 nm.

For the chemical characterization of the components, nanoparticles and films were analyzed by Fourier transform infrared spectroscopy (FTIR). We analyzed the compositions using a spectrophotometer (Model IR PRESTIGE-2, PerkinElmer) with a reading range of 4000–450 cm^{-1} (resolution of 4 cm^{-1}).

In vitro, assays were conducted to evaluate the thermoresponsive release of lidocaine incorporated into PCL-T-based nanoemulsions. The experiment was performed in triplicate. Briefly, 2 mL of PCL-T: LID1%, PCL-T: LID1.5%, or PCL-T: LID2% samples were placed in reconstituted cellulose-based dialysis tubes (SPECTRA/POR, cut-off 3,500 Da), sealed, and placed in test tubes containing 10 mL of 0.3% Tween 80® solution to maintain the sink condition. The tests were conducted at two temperatures, 37 ± 1 ºC and 43 ± 1 ºC, which simulate the temperature of healthy and inflamed skin, respectively [31]. At predetermined time intervals, aliquots of the solution were collected, and the quantification of released lidocaine was determined by UV-vis spectroscopy at a wavelength of 261 nm and using a validated method (as previously described).

2.4 Preparation of alginate/hyaluronic acid film embedded with PCL-T-based nanoemulsion

To obtain the films, solutions containing 5% (v/v) glycerol, 1.5% (w/v) alginate, and 0.5% (w/v) sodium hyaluronate (coded as ALG:AH) were prepared by dissolving them in purified water followed by heating to 50 °C under constant stirring. After complete dissolution, the solution was cooled to room temperature and subsequently diluted in the solution of the nanoemulsions PCL-T:LID1% (coded as ALG:AH@PCL-T:LID1%), PCL-T:LID1.5% (coded as ALG:AH@PCL-T:LID1.5%) and PCL-T:LID2% (coded as ALG:AH@PCL-T:LID2%) in a 1:1 ratio.

The solutions were gently mixed, placed on a Petri dish, and dried in a fume hood at room temperature for 24 h. The crosslinking of the dried films was performed by exposing them for 1 min to a 1% (w/v) calcium chloride solution.

2.5 Characterization of alginate/hyaluronic acid films embedded with PCL-T-based nanoemulsion

Morphological analysis of the ALG:AH@PCL-T:LID1%, ALG:AH@PCL-T:LID1.5%, and ALG:AH@PCL-T:LID2% films was performed using a scanning electron microscope (JEOL JSM-6510) at an accelerating voltage of 10 kV. For this purpose, samples from the surface and fracture of the dried films were packed on aluminum stubs using a carbon tape and coated with a thin layer of gold.

Contact angle analysis was performed using the sessile drop method. An OCA contact angle system from Dataphysics (GmbH instruments) was used for this purpose. A sample of the films was placed on top of a metal apparatus, and a drop of water was placed

on top of the film surface. The image of the meniscus formed by the water drop was captured by a camera, and the contact angle measurement was obtained with OCA and PCA software V.2.1.9.

Mechanical analysis was performed on a Mettler Toledo dynamic mechanical analyzer (DMA 1). Stress-strain curves were obtained with a loading rate of 1 N/min up to 18 N at 30 °C. Samples were cut to approximately ~0.5 mm wide and ~2 mm long.

In vitro assays were performed to evaluate the thermoresponsive release of lidocaine from ALG:AH@PCL-T:LID1%, ALG:AH@PCL-T:LID1.5%, and ALG:AH@PCL-T:LID2% films. 2.25 cm² samples of each film were placed in dialysis tubes containing 0.5 mL of 0.3% Tween 80® solution. The dialysis tubes were sealed and placed in test tubes containing 30 mL of 0.3% Tween 80® solution to maintain sink conditions. The tests were conducted at two temperatures, 37 ± 1 °C and 43 ± 1 °C, which simulate the temperature of healthy and inflamed skin, respectively [31]. At predetermined time intervals, aliquots of the solution were collected for quantification of the lidocaine released, by UV-Vis spectroscopy, using a wavelength of 261 nm and a previously validated method. The assay was performed in duplicate. The cytotoxicity evaluation of the films was conducted using the HaCaT cell line, composed of immortalized aneuploid human keratinocytes. The cells were cultured in polypropylene flasks containing DMEM medium supplemented with 10% fetal bovine serum (FBS) and maintained in a humidified incubator at 37 °C, with 5% CO_2. The films were sterilized under UV light (254 nm) for 30 min and then incubated in DMEM medium to obtain extractions at a concentration of 0.5 mg/mL. Cell suspensions containing 3 × 104 cells/well were prepared by trypsinization (trypsin/EDTA solution) and seeded in 96-well culture plates and maintained under standard conditions. After incubation for 24 h, the confluent cell layer was exposed to the extracts. Negative control cells were maintained under standard conditions, and positive control cells were exposed to 1% hydrogen peroxide for 60 min. The exposure period was 24 h, and then the protein content was determined using the 0.4% sulforhodamine B method. Absorbance was measured in a spectrophotometer at a wavelength of 254 nm (Spectramax M3, USA) and cell morphology was observed under an inverted microscope (Olympus®).

3. Results and Discussion

The anesthetic lidocaine was incorporated into PCL-T-based nanoparticles by the nanoprecipitation method. Macroscopically, Fig. 1a, the emulsions obtained were homogeneous and had the appearance of an opalescent liquid with a light blue color due to the Tyndall effect [32].

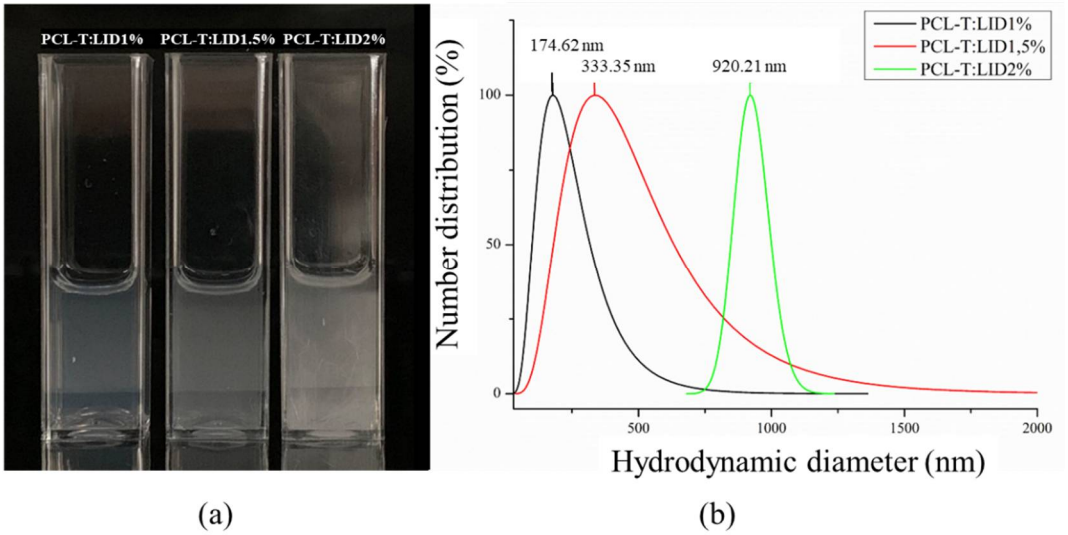

Fig. 1. (**a**) Cuvettes containing samples of PCL-T:LID1%, PCL-T:LID1.5% and PCL-T:LID2% nanoemulsions. (**b**) Particle size dispersion curves in each of the preparations according to DLS analysis.

The apparent diameters of the PCL-T:LID1%, PCL-T:LID1.5% and PCL-T:LID2% samples were predominantly approximately 174, 333 and 920 nm, respectively (Fig. 1b), evidencing a proportional increase with the increase in the concentration of lidocaine incorporated into the nanoparticles. The moderate solubility of lidocaine (logP = 2.56) and PCL-T (logP = 1.9) in water and their chemical characteristics, where lidocaine (Fig. 2c) is present as primary amide (RHNCOR'), tertiary amine (R_2NR') and functional groups of the aliphatic and aromatic hydrocarbon chain, favoring multiple interactions, namely, hydrogen, dipole–dipole and van der Waals bonds, with PCL-T (esters —RCOR', alcohols —OH and hydrocarbon chain). Furthermore, the moderate lipophilicity of lidocaine, superior to that of PCL-T, promotes two scenarios: (1) lidocaine preferentially within the PCL-T matrix and (2) lidocaine also on the surface of PCL-T [30].

The calculated polydispersity indices were 0.296, 0.351 and 0.172 for the PCL-T:LID1%, PCL-T:LID1.5% and PCL-T:LID2% samples, respectively, while the specific zeta potential values were +29.27 mV, +38.89 mV and +49.5 mV, demonstrating that the prepared nanoparticles present relative homogeneity in size, with adequate colloidal stability [33,34], although the PCL-T:LID1.5% sample indicates greater heterogeneity [33].

The zeta potential reported for PCL and lidocaine nanoparticles, of −20.1 ± 0.8 mV, differed from that described by Campos et al. [17], and may have been influenced by the particle composition and dispersing medium, as well as by the pH and ionic strength of the solution. The PCL nanoparticles described by Barbault-Foucher et al. [9] presented a zeta potential of −41 ± 5 mV, which was slightly altered to approximately −43 ± 5 mV after hyaluronic acid adsorption, values significantly different from those observed in the nanoparticles developed in this study. Furthermore, the HA-coated PVA-PCL scaffold described by Fakhraei et al. [35] showed a negative zeta potential (approximately −15 mV), attributed to the ionizable carboxylic groups of HA. Therefore, the positive zeta potential values observed in this work can be attributed to the presence of lidocaine on the surface of the nanoparticles, since studies indicate that the amphiphilic nature of anesthetics such as lidocaine allows them to act as surfactants [34,36].

The encapsulation efficiency of lidocaine incorporated into PCL-T nanoparticles was estimated by the ultrafiltration-centrifugation method, and if any lidocaine is found in the filtered liquid, this refers to the unencapsulated lidocaine fraction [30,37]. The encapsulation efficiency values were greater than 99% for all nanoemulsions prepared in this study. The high encapsulation efficiency of lidocaine is influenced by its low water solubility (3 mg/mL) and its hydrophobic nature (Log P = 2.56), which allows it to interact favorably with PCL-T (Log P = 1.9), the hydrophobic polymer used in encapsulation [13,17]. These properties make lidocaine a suitable candidate for encapsulation in polymeric systems, where it can be effectively entrapped in the polymer matrix. Similar encapsulation efficiency results to PCL-T (900 g/mol) based nanostructures were reported for ritonavir (Log P = 4.3) PCL-T (900 g/mol) based nanostructures [38].

The FTIR spectra of pure PCL-T, lidocaine, and sodium hyaluronate and the lidocaine-loaded nanoparticles (PCL-T:LID1%, PCL-T:LID1.5%, and PCL-T:LID2%) are shown in Fig. 2a,b. FTIR studies were performed to indicate possible interactions and examine the compatibility between the inputs.

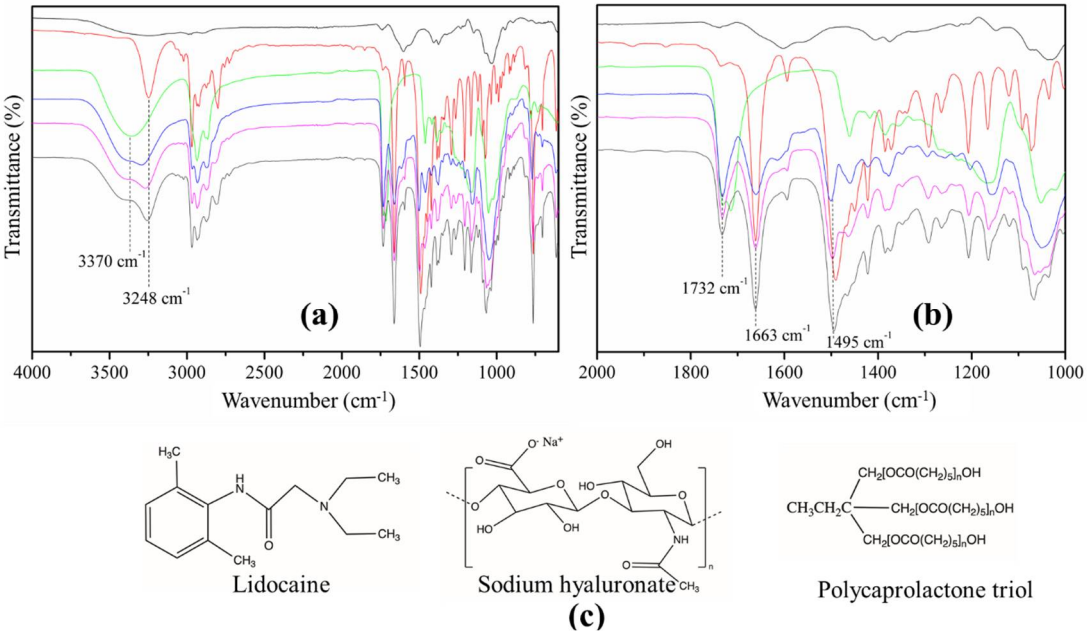

Fig. 2. FTIR spectra of sodium hyaluronate (black line), lidocaine (red line), PCL-T (green line), PCL-T:LID1% (blue line), PCL-T:LID1.5% (magenta line), and PCL-T:LID2% (gray line) between wavenumbers of (**a**) 4000 and 400 cm^{-1} and (**b**) 2000 and 1000 cm^{-1}. (**c**) Chemical structures of lidocaine, PCL-T, and sodium hyaluronate.

Lidocaine, whose structure is shown in Fig. 2c, consists of a main chain that includes an amide group linked to a substituted phenyl ring and a tertiary amine group. The FTIR spectrum, shown in Fig. 2a, shows a characteristic band at 3248 cm^{-1} associated with the NH stretching of the primary amide group (R-NH-CO-R'). In Fig. 2a,b, the bands at 1663 cm^{-1} and 1495 cm^{-1} are associated with the vibration of the C=O and C=C groups, respectively [30,39,40]. In the region of 1600-1450 cm^{-1}, multiple bands of medium intensity indicate the C=C stretching of the aromatic ring, with emphasis on the band near 1580 cm^{-1}, reflecting the complexity of

the 2,6-dimethylphenyl structure. Between 1300-1000 cm^{-1}, the C-N stretching of the tertiary amine ($RN(C_2H_5)_2$) appears with medium intensity, confirming the presence of the diethylamino group.

PCL-T, the structure in Fig. 2c, presents units connected by ester bonds, the presence of three terminal hydroxyl groups and extensive hydrocarbon chains. In the spectrum, Fig. 2a, the broad band observed in the region between 3000 and 3600 cm^{-1} (3370 cm^{-1}) was attributed to the hydroxyl group (OH). In Fig. 2a,b, typical absorption bands with strong intensity at 1732 cm^{-1} of the C=O group vibration can be observed [30,39].

Also in Fig. 2, the FTIR spectrum of sodium hyaluronate presents a broad absorption band in the region between 3000 and 3600 cm^{-1} centered at 3300 cm^{-1} (Fig. 2a) associated with the stretching of the OH groups, present in the D-glucuronate and N-acetyl-D-glucosamine rings. The amide I band, located near 1620 cm^{-1}, corresponds to the stretching of the C=O bond of the acetamido (N-acetyl) group present in N-acetyl-D-glucosamine. In turn, the amide II band, located at 1560 cm^{-1}, is associated with a combination of N-H deformation and C-N stretching of the acetamido group. This band was less intense than amide I, but essential to confirm the presence of the N-acetyl group. Its position and intensity can be influenced by the interaction with sodium ions, which stabilize the ionized structure of the carboxylate ($-COO^-$), widely distributed along the polysaccharide chain [41].

The spectra obtained from the PCL-T:LID1%, PCL-T:LID1.5%, and PCL-T:LID2% samples showed that these are the sum of the spectra of sodium hyaluronate, PCL-T, and lidocaine. The spectral signal of the nanoparticles was presented in Fig. 2a,b, being PCL-T:LID1% (blue line), PCL-T:LID1.5% (magenta line), and PCL-T:LID2% (gray line). Fig. 2a shows the bands at 3370 cm^{-1} and 3248 cm^{-1}, referring to the hydroxyl groups present in the PCL-T and lidocaine molecules, respectively.

In Fig. 2b, the peak at 1732 cm^{-1} (C=O) and the peaks at 1663 cm^{-1} and 1495 cm^{-1} in the spectra indicate stretching corresponding to PCL-T and lidocaine, respectively. For all spectra in Fig. 2b, stretching was observed in the region of 1620–1580 cm^{-1}, which is typical of carbonyl groups, indicating the presence of C=O bonds in the acetamido (N-acetyl of sodium hyaluronate) and C=C bonds in the aromatic ring (lidocaine) [16].

Fig. 3 shows the *in vitro* release profile of lidocaine from the PCL-T nanoparticle, an analysis that was conducted at temperatures of 37 ± 1 °C and 43 ± 1 °C, temperatures that simulate healthy and inflamed skin, respectively.

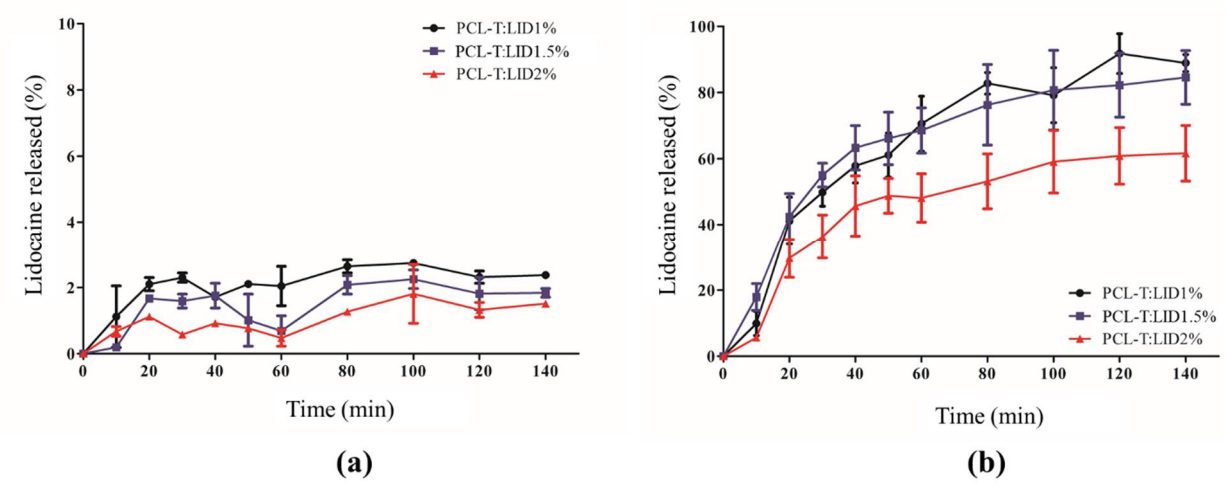

Fig. 3. Percentage of lidocaine released *in vitro* from the nanoemulsions PCL-T:LID1%, PCL-T:LID1.5%, and PCL-T:LID2% at (a) 37 ± 1 °C and (b) 43 ± 1 °C. The assays were performed in triplicate.

The curves presented in Fig. 3 show the relationship between the drug load and the lidocaine release rate from the compositions PCL-T:LID1%, PCL-T:LID1.5% and PCL-T:LID2% in response to increasing time, at temperatures of (a) 37 ± 1 °C and (b) 43 ± 1 °C. In 140 min and at a temperature of 37 °C (Fig. 3a), the percentages of lidocaine released were approximately 2.8%, 2.2% and 1.8% for the compositions PCL-T:LID1%, PCL-T:LID1.5% and PCL-T:LID2%, respectively. On the other hand, at 43 °C, during the same time interval (Fig. 3b), the percentages of lidocaine released *in vitro* reached approximately 91.8% for PCL-T:LID1%, 84.5% for PCL-T:LID1.5%, and 61.64% for PCL-T:LID2%. This difference in the percentage of lidocaine released at different temperatures is possibly related to the physical state of PCL-T at the two experimental temperatures (37 ± 1 °C and 43 ± 1 °C). Considering that PCL-T has a melting point of approximately 33 °C [39], while lidocaine has a melting point of approximately 69 °C [16], the increase in temperature is expected to promote the disaggregation of the nanoparticulate structure of PCL-T, thus favoring a thermoresponsive release of lidocaine [42]. It can also be seen that there was a tendency for a reduction in the percentage of drug release with increasing concentration in the nanoparticle at both temperatures, this effect being particularly evident in the PCL-T:LID2% sample.

One explanation for this relationship considers the possibility of drug crystallization within nanoparticles, which occurs when its concentration exceeds the solubility in the matrix, resulting in slower or incomplete diffusion through polymeric materials [7].

The growing demand for functional materials applicable to tissue engineering and wound care has driven the development of polymeric systems that combine appropriate active and structural properties. Notable among these are natural biopolymers such as alginate (ALG) and hyaluronic acid (HA), widely used in the formulation of hydrogels for topical application. Their intrinsic characteristics of biocompatibility, biodegradability, and ability to form hydrated three-dimensional networks make them excellent matrices for the encapsulation and controlled release of therapeutic agents, in addition to promoting a moist environment conducive to healing. In the present study, these matrices were used as a base for incorporating PCL-T nanoparticles containing lidocaine, with the aim of developing a multifunctional system for wound application. The ALG:AH, ALG:AH@PCL-T:LID1%, ALG:AH@PCL-T:LID1.5%, and ALG:AH@PCL-T:LID2% films showed homogeneity on a macroscopic scale, exhibited high transparency (Fig.4a), and demonstrated ease of manipulation.

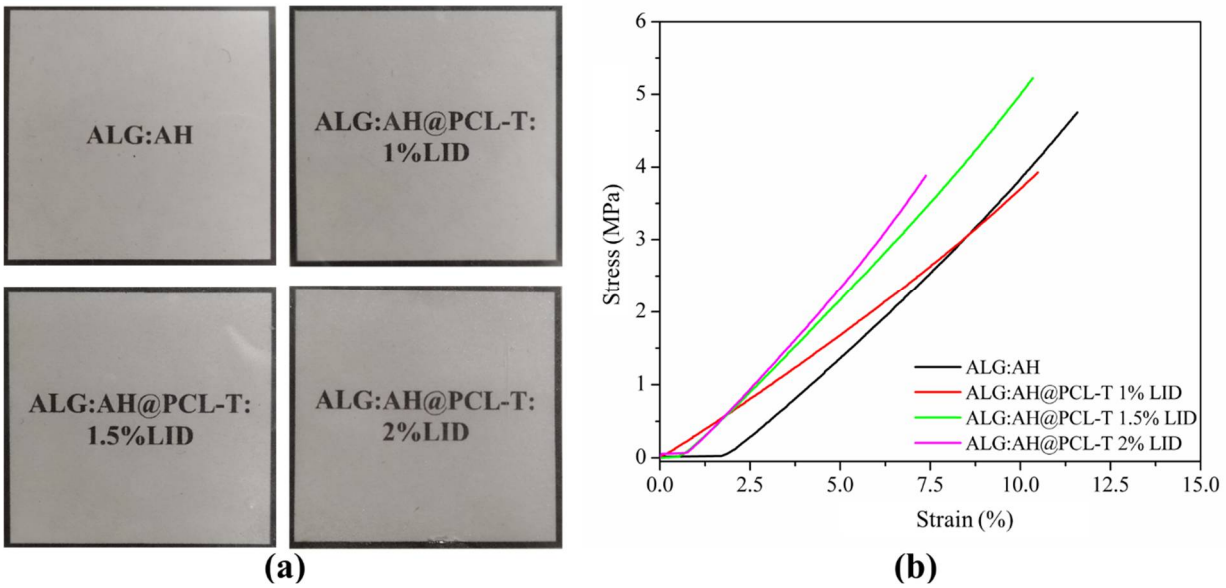

Fig. 4. (**a**) The ALG: AH, ALG:AH@PCL-T: LID1%, ALG:AH@PCL-T: LID1.5% and ALG:AH@PCL-T: LID2% films presented translucent visual appearance. (**b**) Stress-strain curves of the ALG: AH (black line), ALG:AH@PCL-T: LID1% (red line), ALG:AH@PCL-T: LID1.5% (green line), and ALG:AH@PCL-T: LID2% (magenta line) films.

In Fig. 4b, the elastic modulus values calculated from the stress-strain curves were 0.481 MPa, 0.369 MPa, 0.529 MPa, and 1.79 MPa for ALG: AH, ALG:AH@PCL-T: LID1%, ALG:AH@PCL-T: LID1.5%, and ALG:AH@PCL-T: LID2%, respectively. Although the strain values obtained for the films do not exceed 11%, which corresponds to body orientations in the linear elastic deformation zone at low strains (up to 10-40%), the elastic moduli for the samples are close to or within the range reported for human skin, which varies from 0.50 to 1.95 MPa [43]. The ALG: AH film presented an elastic modulus of 0.33 MPa, while the films containing lidocaine presented the following values: 2.68 MPa for ALG:AH@PCL-T: LID1%, 1.93 MPa for ALG:AH@PCL-T: LID1.5% and 1.77 MPa for ALG:AH@PCL-T: LID2%.

Mechanical properties are similar to those of skin are desirable for topical application materials, as they allow the film to maintain its physical integrity during use without causing discomfort, especially in areas with low skin deformation [43,44].

Fig. 5 shows the surface and fracture images obtained by scanning electron microscopy for the ALG:AH, LG:AH@PCL-T:LID1%, ALG:AH@PCL-T:LID1.5%, and ALG:AH@PCL-T:LID2% films at ×1000 magnification.

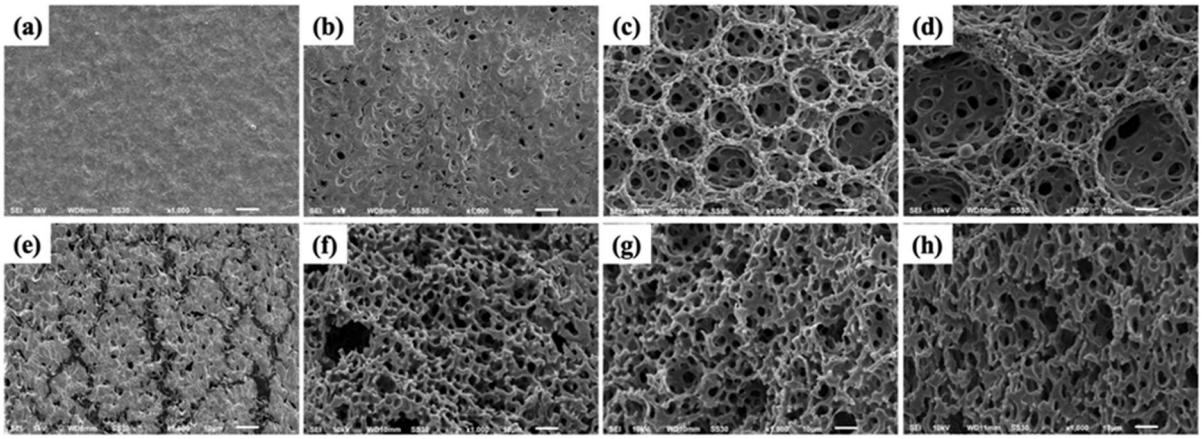

Fig. 5. SEM images of the surfaces (**a–d**) and fractures (**e–h**) of the films: (**a, e**) ALG:AH; (**b, f**) ALG:AH@PCL-T:LID1%; (**c, g**) ALG:AH@PCL-T:LID1.5%; (**d, h**) ALG:AH@PCL-T:LID2%.

In Fig. 5, SEM images of the films reveal a porous structure. It can be observed that the addition of NPs to the films promotes an increase in porosity, both on the surface (Fig. 5a–d) and in the fractured walls (Fig. 5e–h), accompanying the increase in lidocaine concentration in the NPs. In the ALG:AH sample, Fig. 6a, no pores were observed on the surface of the film at ×1000 magnification. However, within the sample (Fig. 5e), pores and striations were observed.

The samples containing nanoparticles (Fig. 5b–d, representing the surface, and Fig. 5f–h, representing the cross section) exhibited a porous morphology with the presence of interconnected pores, a characteristic indicative of a three-dimensional cross-linked structure. This structural organization can be attributed to the interaction between the amine groups (pKa = 8.01) present in the lidocaine molecule and the hydrophilic carboxyl groups (–COOH/–COO^-) of the polymeric chains of alginate (pKa ≈ 3.4-3.6) and sodium hyaluronate (pKa ≈ 2.5-4.0). These interactions can act as additional physical crosslinking points, favoring the formation of a more open and interconnected three-dimensional network. In addition, the presence of lidocaine molecules, particularly on the surface of PCL-T nanoparticles, may lead to microphase domains and discontinuities in the polymeric matrix, contributing to increased porosity. This mechanism is consistent with previous reports [18,44] describing the role of amine-containing drugs as modulators of the microstructure of polysaccharide hydrogels. This potential role of lidocaine as a cross-linking agent contributes to the formation and stabilization of the polymer network, favoring the development of a continuous porous matrix. Similar mechanisms were reported by Jing et al. [44], in studies using lidocaine-loaded carboxymethyl chitosan cross-linked in alginate hydrogels for local anesthetic delivery systems, as well as by Sanchez et al. [18], who described the formation of alginate- and hyaluronate-based ion-exchange films containing ciprofloxacin and lidocaine, with a porous structure and controlled-release profile for use in wound healing. These results reinforce the hypothesis that the presence of lidocaine can influence not only the bioactivity of the system but also its structural and functional properties.

It is established that hydrophilic surface films enhance adhesion to skin through electrostatic interactions [13,16]. Contact angles below 90° indicate hydrophilic interactions between the material surface and the solution, while angles between 90° and 150° suggest hydrophobic interactions [13,45]. To investigate the chemical nature of the films, contact angle analyses were conducted, with results presented in Fig. 6. The same figure also displays FTIR spectra for ALG:AH@PCL-T:LID1%, ALG:AH@PCL-T:LID1.5%, and ALG:AH@PCL-T:LID2% films.

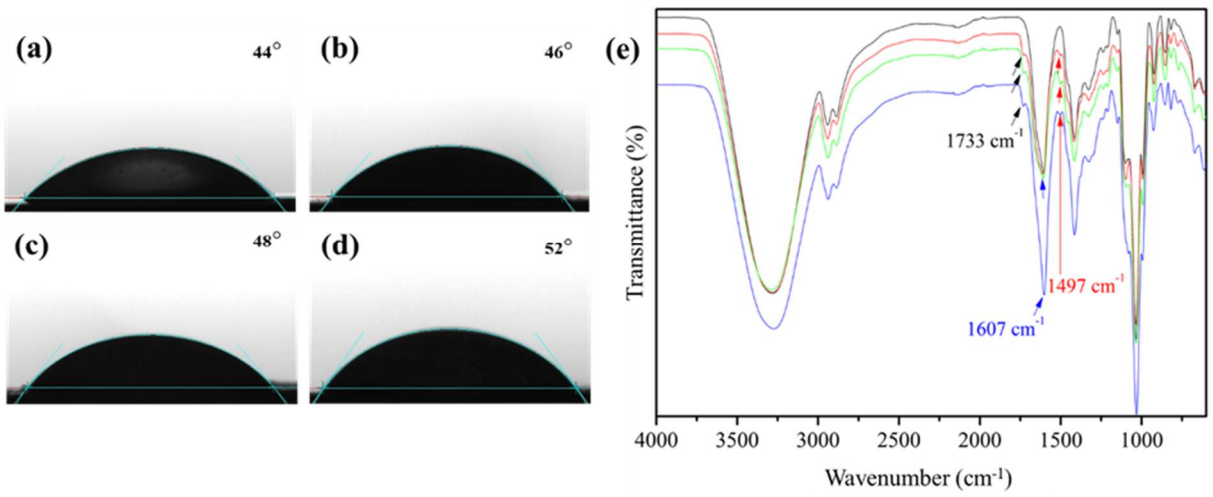

Fig. 6. Calculated Contact Angles for Films (**a**) ALG:AH, (**b**) ALG:AH@PCL-T:LID1%, (**c**) ALG:AH@PCL-T:LID1.5%, and (**d**) ALG:AH@PCL-T:LID2%. (**e**) FTIR Spectra (4000–600 cm^{-1}) for ALG:AH (black line), ALG:AH@PCL-T:LID1% (red line), ALG:AH@PCL-T:LID1.5% (green line), and ALG:AH@PCL-T:LID2% (blue line).

As expected, all contact angle values obtained were less than 90° (Fig. 6a-d), confirming that the films are hydrophilic in nature. However, it is observed that increasing the concentration of lidocaine incorporated into the PCL-T nanoparticles results in an increase in the contact angle, suggesting a tendency toward hydrophobicity. This increase may be due to the presence of lidocaine on the surface of the PCL-T nanoparticles, as discussed previously.

In general, the spectra presented in Fig. 6e exhibit the typical absorption bands of polysaccharides, such as alginate and sodium hyaluronate, characterized by: a broad absorption band between 3000 and 3700 cm^{-1}, associated with the stretching of the OH groups; an intense absorption band centered at 1608 cm^{-1}, related to the stretching of the carbonyl groups present in both compounds; and a band at 1051 cm^{-1}, corresponding to the glycosidic bonds [46]. When comparing the spectra of ALG:AH@PCL-T:LID1%, ALG:AH@PCL-T:LID1.5% and ALG:AH@PCL-T:LID2% with ALG:AH, important differences are observed, including: an absorption band at 1495 cm^{-1}, attributed to the stretching of the C=C group of lidocaine [40], and another at 1733 cm^{-1}, resulting from the vibration of the C=O group present in PCL-T [30,39]. These differences confirm the incorporation of PCL-T-based nanoparticles containing lidocaine in the alginate and sodium hyaluronate films.

The lidocaine release profile from ALG:AH@PCL-T:LID1%, ALG:AH@PCL-T:LID1.5% and ALG:AH@PCL-T:LID2% films at 37 ± 1°C and 43 ± 1°C are shown in Fig. 7.

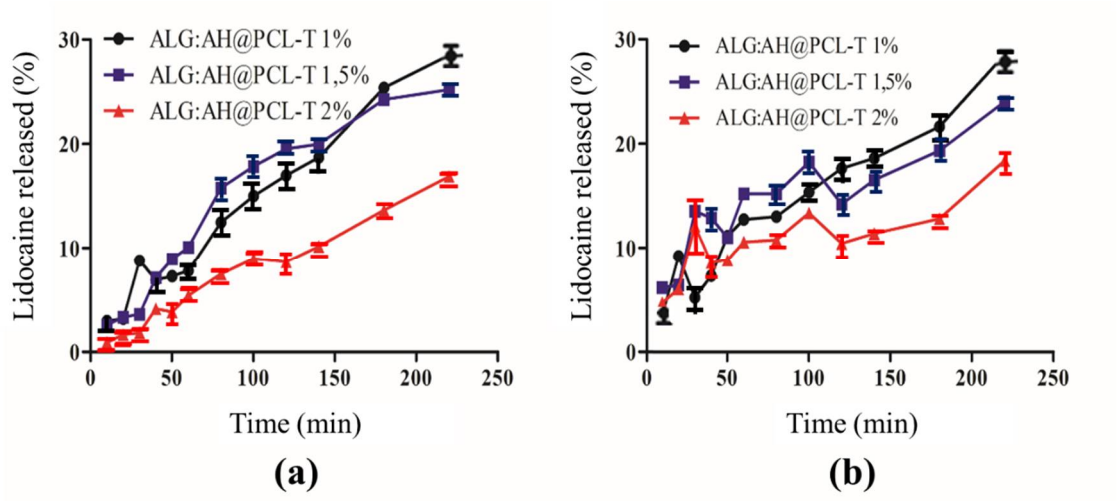

Fig. 7. Percentage of lidocaine released from the films of ALG:AH@PCL-T:LID1%, ALG:AH@PCL-T:LID1.5%, and ALG:AH@PCL-T:LID2% at the temperature of (**a**) 37 ± 1 °C and (**b**) 43 ± 1 °C. The assays were performed in triplicate.

As shown in Fig. 7, the amounts of lidocaine released in 220 min from the membranes were comparable at temperatures of 37 ± 1 °C (Fig. 7a) and 43 ± 1 °C (Fig. 7b). For example, at 37 °C and after 220 min, the amounts of lidocaine released were approximately 28.5% for PCL-T:LID1%, 25.2% for PCL-T:LID1.5%, and 16.9% for PCL-T:LID2%. When the temperature increased to 43 °C, a reduction in the release percentages was observed to 23.8%, 20.0%, and 15.3%, respectively. In comparison, this decrease corresponds to reductions of approximately 16.5%, 20.6%, and 9.5% in lidocaine release for the systems with 1.0%, 1.5%, and 2.0% drug, respectively. These results indicate that increasing the temperature did not favor drug release, suggesting that the release process is not predominantly governed by thermally activated mechanisms, such as matrix degradation, but rather by a controlled diffusion mechanism.

Thus, the low amount of lidocaine released from the membranes at both temperatures studied may be related to the presence of electrostatic interactions between the amine groups of lidocaine and the carboxylic groups present in the polymer chains of alginate and sodium hyaluronate. Such interactions can restrict the mobility of the drug in the matrix, hindering its diffusion into the receptor medium (0.3% Tween 80 solution). This behavior has been previously reported, demonstrating that the use of a neutral salt, such as sodium chloride, as a receptor medium can disrupt these electrostatic interactions and, consequently, significantly increase the lidocaine release rate [18].

Considering the low lidocaine release rate observed in the developed systems, it is essential to assess whether the amount of drug effectively available in the medium is sufficient to promote the desired biological effects, such as local anesthetic action, without inducing cellular toxicity. In this context, cytotoxicity assays are essential to investigate the safety of the systems against human cells. Below, we present the results of the acute toxicity evaluation (24 h) of films containing different concentrations of lidocaine, conducted according to the criteria established by ISO 10993-6:2016, which establishes that a sample is considered cytotoxic when cell viability is less than 70%. Fig. 8 presents the results obtained for the ALG:AH@PCL-T:LID1%, ALG:AH@PCL-T:LID1.5%, and ALG:AH@PCL-T:LID2% films, evaluated against the human keratinocyte cell line HaCat.

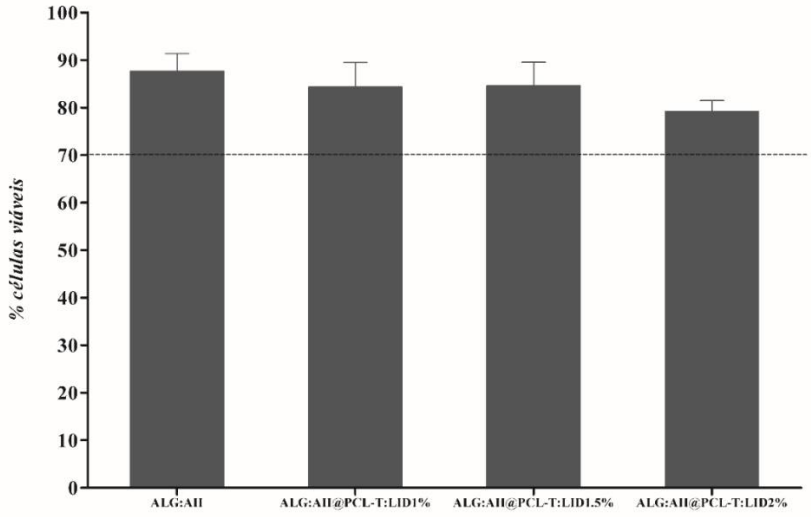

Fig. 8. Cytotoxicity of films against HaCat cell line.

As shown in Fig. 8, all films containing lidocaine – ALG:AH@PCL-T: LID1%, ALG:AH@PCL-T: LID1.5%, and ALG:AH@PCL-T: LID2% – showed cell viability greater than 70%, the limit established by ISO 10993-6:2016 for characterizing cytotoxicity. More precisely, the control film, composed only of ALG: AH, showed an average viability of approximately 88%, while the films containing lidocaine at concentrations of 1.5%, 1.0%, and 2.0% exhibited average viability values of ~85%, ~84%, and ~79%, respectively. These results indicate that all developed systems are biocompatible, demonstrating potential for biomedical applications, especially as matrices for topical delivery of local anesthetics.

5. Conclusions

This study reports on the successful development of innovative topical films based on alginate and hyaluronic acid, loaded with lidocaine-containing polycaprolactone-triol nanoparticles. The prepared nanoparticles, obtained via nanoprecipitation, demonstrated hydrodynamic diameters ranging from 174 to 920 nm, high encapsulation efficiency (>99%), and good colloidal stability. The final films were characterized by their flexibility, translucency, and mechanical properties comparable to human skin, with a porous morphology facilitated by intermolecular interactions between the drug and the matrix biopolymers.

While the isolated nanoparticles exhibited a thermoresponsive release profile, with enhanced release at an elevated temperature (43 °C) simulating inflamed skin, this effect was attenuated in the final film formulation. This suggests that electrostatic interactions between lidocaine and the polyanionic matrix limited drug diffusion. Nevertheless, the films demonstrated a sustained release profile, releasing approximately 28.5% of the encapsulated drug over 220 minutes under physiological conditions.

HaCaT cell viability assays confirmed the biocompatibility of all developed formulations, with cell viability exceeding 79%. These results underscore the potential of the films for biomedical applications, particularly as intelligent dressings for prolonged pain relief and wound healing. Although *in vivo* therapeutic efficacy remains to be fully explored, this work establishes a robust foundation for future studies. Subsequent investigations will focus on evaluating the analgesic and healing properties of these films in animal models and exploring the potential for simultaneous release of multiple drugs to further expand their clinical utility.

Author Contributions: Conceptualization, K. M. Zepon; methodology, K. M. Zepon, R. F. Magnago and L. A. Kanis; formal analysis, K. M. Zepon, and R. F. Magnago; investigation, D. P. Darella, T. V. Joaquim and F. M. Moraes; resources, M. Maraschin; writing—original draft preparation, D. P. Darella and T. V. Joaquim and; writing—review and editing and K. M. Zepon, R. F. Magnago; supervision, K. M. Zepon. All authors have read and agreed to the published version of the manuscript.

Funding: This research did not receive external funding.

Informed Consent Statement: Not applicable.

Data Availability Statement: Not applicable.

Acknowledgments: The authors thank the University of Southern Santa Catarina, Feevale University and Federal University of Santa Catarina for their support and infrastructure.

Conflicts of Interest: The authors declare no conflict of interest.

References

1. Alcântara, M.T.S.; Lincopan, N.; Santos, P.M.; Ramirez, P.A.; Brant, A.J.C.; Riella, H.G.; Lugão, A.B. Simultaneous Hydrogel Crosslinking and Silver Nanoparticle Formation by Using Ionizing Radiation to Obtain Antimicrobial Hydrogels. *Radiat. Phys. Chem.* **2019**, *165*, 108369. https://doi.org/10.1016/j.radphyschem.2019.108369
2. Lin, C.-C.; Metters, A.T. Hydrogels in Controlled Release Formulations: Network Design and Mathematical Modeling. *Adv. Drug Deliv. Rev.* **2006**, *58*, 1379–1408. https://doi.org/10.1016/j.addr.2006.09.004.
3. Bustamante-Torres, M.; Romero-Fierro, D.; Arcentales-Vera, B.; Palomino, K.; Magaña, H.; Bucio, E. Hydrogels Classification According to the Physical or Chemical Interactions and as Stimuli-Sensitive Materials. *Gels* **2021**, *7*, 182. https://doi.org/10.3390/gels7040182.
4. Uhrich, K.E.; Cannizzaro, S.M.; Langer, R.S.; Shakesheff, K.M. Polymeric Systems for Controlled Drug Release. *Chem. Rev.* **1999**, *99*, 3181–3198. https://doi.org/10.1021/cr940351u
5. Campea, M.A.; Majcher, M.J.; Lofts, A.; Hoare, T. A Review of Design and Fabrication Methods for Nanoparticle Network Hydrogels for Biomedical, Environmental, and Industrial Applications. *Adv. Funct. Mater.* **2021**, *31*, 2102355. https://doi.org/10.1002/adfm.202102355
6. Malik, S.; Muhammad, K.; Waheed, Y. Emerging Applications of Nanotechnology in Healthcare and Medicine. *Molecules* **2023**, *28*, 6624. https://doi.org/10.3390/molecules28186624
7. Castro, K.C. de; Costa, J.M.; Campos, M.G.N. Drug-Loaded Polymeric Nanoparticles: A Review. *Int. J. Polym. Mater. Polym. Biomater.* **2022**, *71*, 1–13. https://doi.org/10.1080/00914037.2020.1798436
8. Erdoğar, N.; Akkın, S.; Bilensoy, E. Nanocapsules for Drug Delivery: An Updated Review of the Last Decade. *Recent Pat. Drug Deliv. Formul.* **2018**, *12*, 252–266. https://doi.org/10.2174/1872211313666190123153711
9. Barbault-Foucher, S.; Gref, R.; Russo, P.; Guechot, J.; Bochot, A. Design of Poly-ε-Caprolactone Nanospheres Coated with Bioadhesive Hyaluronic Acid for Ocular Delivery. *J. Control. Release* **2002**, *83*, 365–375..
10. Fessi, H.; Puisieux, F.; Devissaguet, J.P.; Ammoury, N.; Benita, S. Nanocapsule Formation by Interfacial Polymer Deposition Following Solvent Displacement. *Int. J. Pharm.* **1989**, *55*, R1–R4. https://doi.org/10.1016/0378-5173(89)90281-0
11. Kumari, L.; Choudhari, Y.; Patel, P.; Gupta, G.D.; Singh, D.; Rosenholm, J.M.; Bansal, K.K.; Kurmi, B.D. Advancement in Solubilization Approaches: A Step towards Bioavailability Enhancement of Poorly Soluble Drugs. *Life* **2023**, *13*, 1099. https://doi.org/10.3390/life13051099
12. Mirchandani, Y.; Patravale, V.B.; Brijesh, S. Solid Lipid Nanoparticles for Hydrophilic Drugs. *J. Control. Release* **2021**, *335*, 457–464. https://doi.org/10.1016/j.jconrel.2021.05.032
13. Silva, A.; Mourão, J.; Vale, N. A Review of the Lidocaine in the Perioperative Period. *J. Pers. Med.* **2023**, *13*, 1699. https://doi.org/10.3390/jpm13121699

14. Arumugam, S.; Contino, V.; Kolli, S. Local Anesthetic Systemic Toxicity (LAST)—A Review and Update. *Curr. Anesthesiol. Rep.* **2020**, *10*, 218–226.
15. El-Boghdadly, K.; Pawa, A.; Chin, K.J. Local Anesthetic Systemic Toxicity: Current Perspectives. *Local Reg. Anesth.* **2018**, *11*, 35–44.
16. Muniz, B.V.; Baratelli, D.; Di Carla, S.; Serpe, L.; da Silva, C.B.; Guilherme, V.A.; Ribeiro, L.N. de M.; Cereda, C.M.S.; de Paula, E.; Volpato, M.C.; et al. Hybrid Hydrogel Composed of Polymeric Nanocapsules Co-Loading Lidocaine and Prilocaine for Topical Intraoral Anesthesia. *Sci. Rep.* **2018**, *8*, 17972. https://doi.org/10.1038/s41598-018-36382-4
17. Campos, E.V.R.; Silva de Melo, N.F.; Guilherme, V.A.; de Paula, E.; Rosa, A.H.; de Araújo, D.R.; Fraceto, L.F. Preparation and Characterization of Poly(ε-Caprolactone) Nanospheres Containing the Local Anesthetic Lidocaine. *J. Pharm. Sci.* **2013**, *102*, 215–226. https://doi.org/10.1002/jps.23350
18. Sanchez, M.F.; Guzman, M.L.; Apas, A.L.; Alovero, F. del L.; Olivera, M.E. Sustained Dual Release of Ciprofloxacin and Lidocaine from Ionic Exchange Responding Film Based on Alginate and Hyaluronate for Wound Healing. *Eur. J. Pharm. Sci.* **2021**, *161*, 105789. https://doi.org/10.1016/j.ejps.2021.105789
19. Samiraninezhad, N.; Asadi, K.; Rezazadeh, H.; Gholami, A. Using Chitosan, Hyaluronic Acid, Alginate, and Gelatin-Based Smart Biological Hydrogels for Drug Delivery in Oral Mucosal Lesions: A Review. *Int. J. Biol. Macromol.* **2023**, *252*, 126448. https://doi.org/10.1016/j.ijbiomac.2023.126448
20. Chin, C.Y.; Gan, J.E. Formulation and Characterisation of Alginate Hydrocolloid Film Dressing Loaded with Gallic Acid for Potential Chronic Wound Healing. *F1000Res.* **2021**, *10*, 451. https://doi.org/10.12688/f1000research.52528.1
21. Cui, R.; Zhang, L.; Ou, R.; Xu, Y.; Xu, L.; Zhan, X.Y.; Li, D. Polysaccharide-Based Hydrogels for Wound Dressing: Design Considerations and Clinical Applications. *Front. Bioeng. Biotechnol.* **2022**, *10*, 845735. https://doi.org/10.3389/fbioe.2022.845735
22. Łabowska, M.B.; Michalak, I.; Detyna, J. Methods of Extraction, Physicochemical Properties of Alginates and Their Applications in Biomedical Field—A Review. *Open Chem.* **2019**, *17*, 738–762. https://doi.org/10.1515/chem-2019-0077
23. Rahman, M.M.; Shahid, M.A.; Hossain, M.T.; Sheikh, M.S.; Rahman, M.S.; Uddin, N.; Rahim, A.; Khan, R.A.; Hossain, I. Sources, Extractions, and Applications of Alginate: A Review. *Discov. Appl. Sci.* **2024**, *6*, 443.
24. Fooladi, S.; Nematollahi, M.H.; Rabiee, N.; Iravani, S. Bacterial Cellulose-Based Materials: A Perspective on Cardiovascular Tissue Engineering Applications. *ACS Biomater. Sci. Eng.* **2023**, *9*, 2949–2969.
25. Sodhi, H.; Panitch, A. Glycosaminoglycans in Tissue Engineering: A Review. *Biomolecules* **2021**, *11*, 29. https://doi.org/10.3390/biom11010029
26. Faverzani Magnago, R.; Carolina de Aguiar, A.; Fagundes Valezan, I.; Mendes de Moraes, F.; Luiza Ziulkoski, A.; Dal Pont Morisso, F.; Alberto Kanis, L.; Modolon Zepon, K. Polycaprolactone Triol-Based Polyurethane Film Conjugated Ibuprofen to Sustained Release: Synthesis, Physicochemical, Cytotoxic, and Release Studies. *Eur. Polym. J.* **2022**, *179*, 111533. https://doi.org/10.1016/j.eurpolymj.2022.111533
27. Abbasnezhad, N.; Zirak, N.; Shirinbayan, M.; Kouidri, S.; Salahinejad, E.; Tcharkhtchi, A.; Bakir, F. Controlled Release from Polyurethane Films: Drug Release Mechanisms. *J. Appl. Polym. Sci.* **2021**, *138*, 50083. https://doi.org/10.1002/app.50083
28. Yang, J.; Van Lith, R.; Baler, K.; Hoshi, R.A.; Ameer, G.A. A Thermoresponsive Biodegradable Polymer with Intrinsic Antioxidant Properties. *Biomacromolecules* **2014**, *15*, 3942–3952. https://doi.org/10.1021/bm5010004
29. Dehghanpour, H.R.; Parvin, P.; Younesi, A.; Gilaki, M. Effect of Agitation Methods on Characteristics of Iron Ferrite Nanoparticles Synthesized by Co-Precipitation Process. *Appl. Funct. Mater.* **2022**, *2*, 37–41.
30. Lima, A.S.; Prophiro, J.S.; Zepon, K.M.; Morisso, F.D.P.; de Moraes, F.M.; Ziulkoski, A.L.; da Silva, L.; Magnago, R.F. Polycaprolactone Triol-Based Polyurethane Nanocapsules: High-Efficiency Encapsulation and Sustained Release of Piperine with Enhanced Compatibility. *Polym. Bull.* **2025**, *82*, 1685–1704. https://doi.org/10.1007/s00289-024-05598-y
31. Pham, S.H.; Choi, Y.; Choi, J. Stimuli-Responsive Nanomaterials for Application in Antitumor Therapy and Drug Delivery. *Pharmaceutics* **2020**, *12*, 630. https://doi.org/10.3390/pharmaceutics12070630
32. Johnstone, T.C.; Lippard, S.J. The Effect of Ligand Lipophilicity on the Nanoparticle Encapsulation of Pt(IV) Prodrugs. *Inorg. Chem.* **2013**, *52*, 9915–9920. https://doi.org/10.1021/ic4010642
33. Rodriguez-Loya, J.; Lerma, M.; Gardea-Torresdey, J.L. Dynamic Light Scattering and Its Application to Control Nanoparticle Aggregation in Colloidal Systems: A Review. *Micromachines* **2024**, *15*, 223.
34. Sarheed, O.; Dibi, M.; Ramesh, K.V.R.N.S. Studies on the Effect of Oil and Surfactant on the Formation of Alginate-Based O/W Lidocaine Nanocarriers Using Nanoemulsion Template. *Pharmaceutics* **2020**, *12*, 1223. https://doi.org/10.3390/pharmaceutics12121223
35. Fakhraei, O.; Rostamani, H.; Aliebrahim Nosh Abad, A.; Valizadeh, S.; Bakhshayeshi, M.M.; Rafienia, M. Enhanced Biological Properties of Polyvinyl Alcohol-Polycaprolactone/Hyaluronic Acid-Coated Electrospun Scaffolds for Articular Cartilage Regeneration. *J. Biomater. Sci. Polym. Ed.* **2025**, *36*, 919–942. https://doi.org/10.1080/09205063.2025.2492462
36. Romeo, M.; Hafidi, Z.; Muzzalupo, R.; Pons, R.; García, M.T.; Mazzotta, E.; Pérez, L. Antimicrobial and Anesthetic Niosomal Formulations Based on Amino Acid-Derived Surfactants. *Molecules* **2024**, *29*, 2843. https://doi.org/10.3390/molecules29122843

37. Santos, R.B. dos; Nakama, K.A.; Pacheco, C.O.; de Gomes, M.G.; de Souza, J.F.; de Souza Pinto, A.C.; de Oliveira, F.A.; da Fonseca, A.L.; Varotti, F.; Fajardo, A.R.; et al. Curcumin-Loaded Nanocapsules: Influence of Surface Characteristics on Technological Parameters and Potential Antimalarial Activity. *Mater. Sci. Eng. C* **2021**, *118*, 111356. https://doi.org/10.1016/j.msec.2020.111356
38. Prebianca, G.; Marques, M.S.; Bianchin, M.D.; Contri, R.V.; Külkamp-Guerreiro, I.C. Improved Sensory Properties of a Nanostructured Ritonavir Suspension with a Pediatric Administration Perspective. *Pharm. Dev. Technol.* **2020**, *25*, 1188–1191. https://doi.org/10.1080/10837450.2020.1805762
39. Meier, M.M.; Kanis, L.A.; de Lima, J.C.; Pires, A.T.N.; Soldi, V. Poly(Caprolactone Triol) as Plasticizer Agent for Cellulose Acetate Films: Influence of the Preparation Procedure and Plasticizer Content on the Physico-Chemical Properties. *Polym. Adv. Technol.* **2004**, *15*, 593–600. https://doi.org/10.1002/pat.517
40. Nafisi, S.; Samadi, N.; Houshiar, M.; Maibach, H.I. Mesoporous Silica Nanoparticles for Enhanced Lidocaine Skin Delivery. *Int. J. Pharm.* **2018**, *550*, 325–332. https://doi.org/10.1016/j.ijpharm.2018.08.004
41. Haxaire, K.; Maréchal, Y.; Milas, M.; Rinaudo, M. Hydration of Polysaccharide Hyaluronan Observed by IR Spectrometry. I. Preliminary Experiments and Band Assignments. *Biopolymers* **2003**, *72*, 10–20. https://doi.org/10.1002/bip.10245
42. Abrisham, M.; Noroozi, M.; Panahi-Sarmad, M.; Arjmand, M.; Goodarzi, V.; Shakeri, Y.; Golbaten-Mofrad, H.; Dehghan, P.; Seyfi Sahzabi, A.; Sadri, M.; et al. The Role of Polycaprolactone-Triol (PCL-T) in Biomedical Applications: A State-of-the-Art Review. *Eur. Polym. J.* **2020**, *131*, 109701. https://doi.org/10.1016/j.eurpolymj.2020.109701
43. Yu, B.; Kang, S.Y.; Akthakul, A.; Ramadurai, N.; Pilkenton, M.; Patel, A.; Nashat, A.; Anderson, D.G.; Sakamoto, F.H.; Gilchrest, B.A.; et al. An Elastic Second Skin. *Nat. Mater.* **2016**, *15*, 911–918. https://doi.org/10.1038/nmat4635
44. Jing, X.; Feng, P.; Chen, Z.; Xie, Z.; Li, H.; Peng, X.F.; Mi, H.Y.; Liu, Y. Highly Stretchable, Self-Healable, Freezing-Tolerant, and Transparent Polyacrylic Acid/Nanochitin Composite Hydrogel for Self-Powered Multifunctional Sensors. *ACS Sustain. Chem. Eng.* **2021**, *9*, 9209–9220. https://doi.org/10.1021/acssuschemeng.1c00949
45. Yarce, C.J.; Pineda, D.; Correa, C.E.; Salamanca, C.H. Relationship between Surface Properties and in Vitro Drug Release from a Compressed Matrix Containing an Amphiphilic Polymer Material. *Pharmaceuticals* **2016**, *9*, 34. https://doi.org/10.3390/ph9030034
46. Flores-Garay, K.A.; Martínez-Luévanos, A.; Cruz-Ortiz, B.R.; García-Cerda, L.A.; López-Badillo, C.M. Synthesis of Calcium Silicates by Pechini Method and Exchanging Ions of Sodium Alginate-Calcium Chloride. *Bol. Soc. Esp. Ceram. Vidr.* **2016**, *55*, 239–245. https://doi.org/10.1016/j.bsecv.2016.05.002